Forecasting induced seismicity

Principal Investigator: Jean-Philippe Avouac

Abstract

We investigated the relationship between effective stress variations and seismicity induced by fluid injection or extraction for geothermal energy and gas production. We used the case example of Groningen, where seismicity is induced by gas production, to develop and validate a framework which allows calculating effective stress variations and forecast seismicity. We have explored the applicability of this approach to geothermal sites, focusing on two case examples of geothermal plants in California at Brawley (Imperial valley) and Coso (Owens Valley). Based on thermo-mechanical modelling and the analysis of seismicity and surface deformation we find that in both cases thermal effects play a major role in driving deformation, aseismic fault slip and seismicity. A major finding is that thermal stresses seem to explain the gap of aftershocks at Coso following the Ridgecrest earthquake.

Introduction

There is great need for a better understanding of how seismicity relates to geo-energy production, whether fossil fuels or geothermal energy. Induced and triggered earthquakes have indeed been an impediment to the development of Enhanced Geothermal Systems for geothermal energy production. In addition, there is rising concern for the hazard posed by injection of wastewater from unconventional oil & gas production, and there is only limited understanding of how seismicity relates [*Ellsworth*, 2013; *Elsworth et al.*, 2016; *Goebel et al.*, 2017a; *Goebel et al.*, 2017b; *Goebel and Brodsky*, 2018; *Grigoli et al.*, 2018; *Kim et al.*, 2018]. As part of this project, we have investigated in more depth the relationship between seismicity and effective stress variations in different contexts. We used the seismicity induced by gas production at Groningen (Netherlands) to develop and validate a method to forecast seismicity. We have started adapting it to the case of seismicity induced by geothermal energy production using case examples from California. We summarize below the results obtained so far, which are presented in details in two manuscripts to be submitted soon.

Overview of results on the induced seismicity at Groningen

The Groningen gas field, situated in the north-east of the Netherlands (Figure 1) has been in production since 1963 [e.g., *Bourne et al.*, 2014]. No seismicity had been documented there prior to gas extraction. Small magnitude earthquakes were detected starting in 1990. The seismicity is thought to be due to strain induced by the decrease of the bulk reservoir volume [*e.g.*, *Bourne et al.*, 2015]. Progressive fluid extraction from this reservoir has lead to a significant decrease in reservoir pore fluid. The resulting increase in the effective vertical stress has driven compaction of the reservoir, manifested in subsidence of the ground surface. In a previous study [*Smith et al.*, 2019], we combined InSAR and geodetic (leveling and GPS) data to determine the time evolution of compaction and the relation to pore pressure within the reservoir (Figure 1). Relocation of the seismicity using a

waveform coalescence technique shows that most earthquakes concentrate in the anhydrite caprock. The calculation of the Coulomb stress changes in the caprock due to the reservoir compaction does indeed show a reasonable correlation with the observed seismicity (Figure 1c). We next use a simple Coulomb failure model to model the temporal evolution of seismicity. The model has two-parameters: one parameter is the distance from failure at the time of the onset of gas extraction and the other is the seismicity index defined as the number of earthquakes per unit area and per MPa of coulomb stress increase, once the threshold is exceeded. We use a MCMC technique to determine the pdf of the model parameters. This simple Coulomb failure model, which neglects the effect of earthquake nucleation, fits the time evolution of seismicity remarkably well (Figure 1d). The model also predicts an expected maximum magnitude which increases gradually with time and follows quite closely the observations.

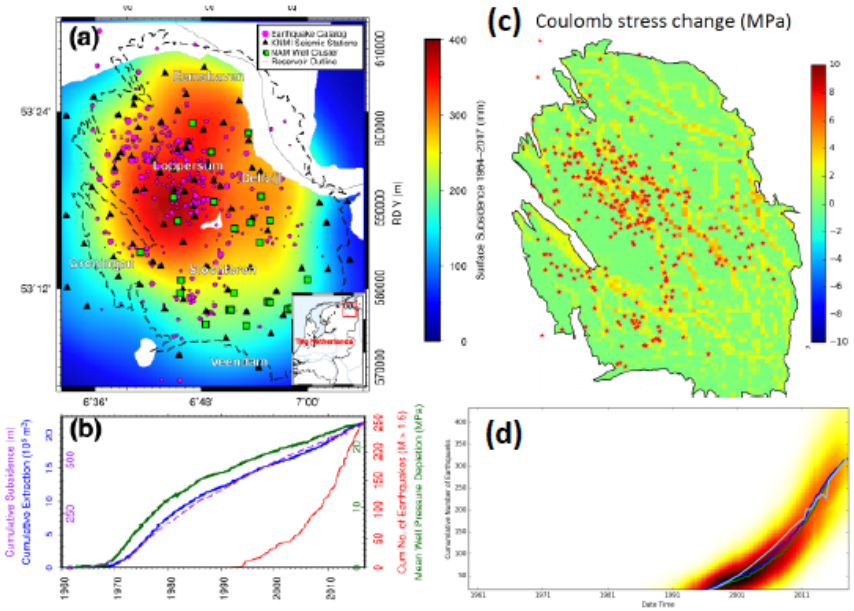

Figure 1: Subsidence, seismicity, cumulative extraction and pressure depletion at Groningen. (a) Surface subsidence between 1964-2017 [*Smith et al.*, 2019]. Seismicity between 1964-2017 shown by pink circles with size scaled by magnitude. Well cluster locations shown by green squares. Gas extent within the reservoir shown black dashed outline. (b) Time evolution of the cumulative subsidence, cumulative extraction, cumulative number of earthquakes, and mean well pressure depletion determined across all well clusters. (c) Comparison between the observed seismicity (red stars) and the cumulative Coulomb stress change in the reservoir caprock since the onset of gas production. (d) Green line shows cumulative number of earthquakes with M_L >1.5 (data source: KMI), and the blue lines show the model prediction using the pore pressure distribution using either the well pressure data (dark blue) or only based on compaction inverted from surface subsidence (light blue). The model assumes a Coulomb stress initially 10 MPa away from failure which was adjusted manually. The other adjustable parameter of the model is the seismicity index (the number of earthquakes per unit area and per MPa of Coulomb stress change).

Induced seismicity related to geothermal operations in California.

To test if the framework developed for Gronigen is transportable, we analysed seismicity and deformation related to the Brawley and Coso geothermal plants in California. An intense seismic crisis occurred in 2012 at Brawley, including a Mw 5.4 earthquake, which started over two years after the onset of energy production (Figure 3). Analysis of InSAR and geodetic data revealed that this earthquake was preceded and triggered by aseismic

motion of a normal fault [*Wei et al.*, 2015]. Because thermal contraction is significant in this context, we modeled the response of the system to fluid injection using a thermo-hydro-mechanical simulation. The simulations will be conducted by Tough-FLAC coupled simulator [*Rutqvist*, 2011] (Figures 2 & 3). The modeled reservoir has two injection wells and four production wells near and across the fault plane.

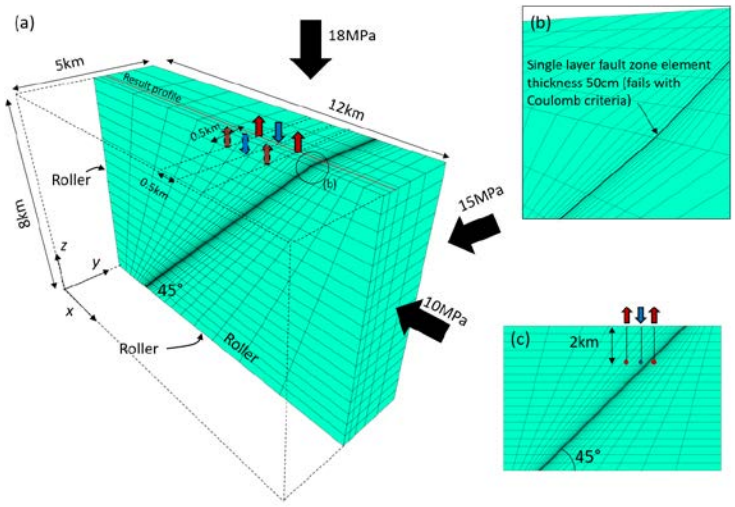

Figure 2: (a) Model geometry. A half of a total 12 km × 5 km × 8 km reservoir domain is depicted. We consider two injection wells and four production wells at 2 km depth. Constant stress boundary conditions with principal stresses of 10 MPa, 15 MPa and 18 MPa along x, y and z, respectively. (b) The fault zone is represented by 50 cm thick elements obeying the Coulomb-Mohr criteria with friction angle 30°. (c) *x*-*z* section. An injector and one producer is located on the hanging wall of the fault, whereas the other producer is located in the footwall, which makes fluid flow across the fault.

Figure 3 presents the time evolution of surface vertical displacement, showing significant subsidence in response to subsurface thermal contraction. More than 10 cm of surface rupture is induced at the end of simulation (Figure 3). Our modelling shows that aseismic fault slip and thermal stresses both contributed to increase the Coulomb stress of the right-lateral fault that eventually ruptured during the 5.4 events at a ~7km depth. The modeling thus succeeds in demonstrating quantitatively how this earthquake, and its foreshocks relate to the geothermal injections at Brawley.

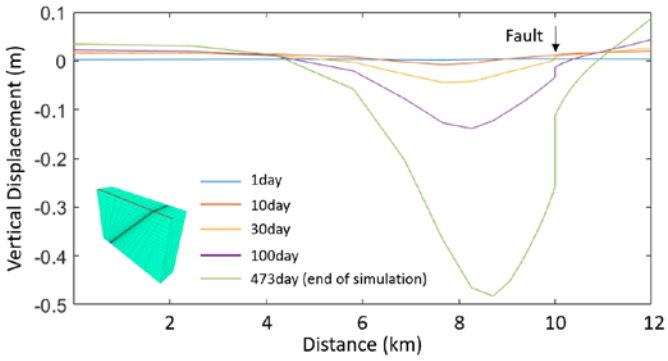

Figure 3: Simulation result. Vertical displacement on the surface (red line, inset) with time.

The Coso geothermal field lies just North of the ruptures of the 2019 Ridgecrest earthquakes. A striking feature of the distribution of aftershocks is the lack of aftershocks within the geothermal field area (rectangle and inset; triangles show location of geothermal wells in Figure 4) where the static Coulomb stress increased as a result of the mainshocks. This observation is surprising as hydrothermal areas

are known to be prone to remote triggering [e.g., Hill, 1993; Brodsky and Prejean, 2005] and that geothermal operations are known to trigger earthquakes [*e.g.*, Deichmann and Giardini, 2009; Grigoli et al., 2018; Kim et al., 2018]. This observation is however consistent with a previous investigation which revealed a lack of remote triggering in that same area [Zhang et al, 2018]. Thermal stresses evolve slowly, and as they accumulate, they can eventually become significant and result in failure and reduction of the deviatoric stresses [Im et al., 2017]. We indeed found through thermo-mechanical modeling that thermal contraction at over the 30 years of production at Coso can have led to a near complete shear stress depletion. While thermal contraction of the reservoir initially induced significant seismicity (Figure 4D), as commonly observed at geothermal sites [Deichmann & Giardini, 2009; Kim et al., 2018], it eventually contributed to deplete the stress available to drive the Ridgecrest aftershock. This mechanism can thus explain both the lack of aftershocks following the 2019 Ridgecrest earthquake and the lack of remotely triggered earthquakes in recent years [Zhang et al., 2017]. We conclude that geothermal heat production at Coso depleted shear stresses within the geothermal reservoir, with this destressing impeding aftershock triggering and possibly arresting the northward propagation of the rupture during the M7.1 mainshock.

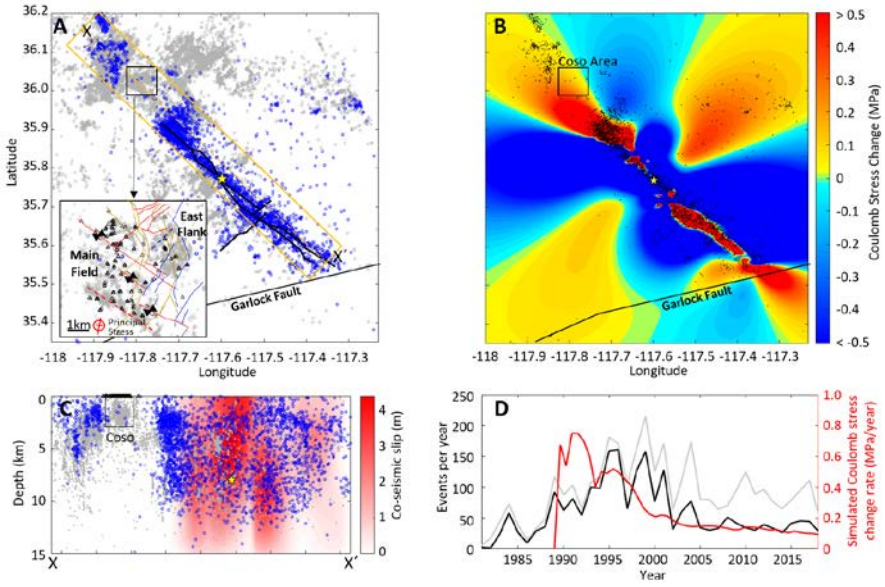

Figure 4. A: Seismicity before and after the 2019 Mw 7.1 Ridgecrest mainshock. Blue circles denote 20 days of aftershocks (M>2; USGS, earthquake.usgs.gov), yellow star denotes epicenter of M7.1 earthquake, black line denotes fault geometry of Ridgecrest earthquakes, gray circles denote relocated seismicity during 1981 – 2017 (M>1). Note the gap of aftershocks around Coso despite the high seismicity prior to 2019. Inset: zoomed-in view of the Coso geothermal field.. **B:** Static Coulomb stress change for right-lateral fault parallel to the main right-lateral fault (red fault in Fig.1 inset) due to the Mw 7.1 2019 events assuming a coefficient of friction 0.6. Dots denote Ridgecrest aftershocks (M>2). **C:** Depth distribution of earthquakes of section XX' in panel A (all events in orange box) with co-seismic slip distribution (red area). **D:** Coulomb stress rate at the center of the reservoir due to thermal contraction and brittle failure of the reservoir compared with seismicity rate around Coso.

References

Bourne, S. J., S. J. Oates, J. J. Bommer, B. Dost, J. van Elk, and D. Doornhof (2015), Monte Carlo Method for Probabilistic Hazard Assessment of Induced Seismicity due to Conventional Natural Gas Production, *Bulletin of the Seismological Society of America*, *105*(3), 1721-1738.

Brodsky, E. E., & Prejean, S. G. (2005). New constraints on mechanisms of remotely triggered seismicity at Long Valley Caldera. *Journal of Geophysical Research: Solid Earth*, *110*(B4). https://doi.org/doi:10.1029/2004JB003211.

Dempsey, D., and J. Suckale (2017), Physics-based forecasting of induced seismicity at Groningen gas field, the Netherlands, *Geophysical Research Letters*, *44*(15), 7773-7782.

Deichmann, N., and D. Giardini (2009), Earthquakes Induced by the Stimulation of an Enhanced Geothermal System below Basel (Switzerland), *Seismological Research Letters*, *80*(5), 784-798.

Ellsworth, W. L. (2013), Injection-Induced Earthquakes, *Science*, *341*(6142), 142-+.

Elsworth, D., Y. Fang, Q. Gan, K. J. Im, T. Ishibashi, and Y. Guglielmi (2016), *Induced seismicity in the development of EGS-benefits and drawbacks*, 13-24 pp.

Goebel, T. H. W., M. Weingarten, X. Chen, J. Haffener, and E. E. Brodsky (2017b), The 2016 Mw5.1 Fairview, Oklahoma earthquakes: Evidence for long-range poroelastic triggering at > 40 km from fluid disposal wells, *Earth and Planetary Science Letters*, *472*, 50-61.

Goebel, T. H. W., and E. E. Brodsky (2018), The spatial footprint of injection wells in a global compilation of induced earthquake sequences, *Science*, *361*(6405), 899-903.

Grigoli, F., S. Cesca, A. P. Rinaldi, A. Manconi, J. A. Lopez-Comino, J. F. Clinton, R. Westaway, C. Cauzzi, T. Dahm, and S. Wiemer (2018), The November 2017 M-w 5.5 Pohang earthquake: A possible case of induced seismicity in South Korea, *Science*, *360*(6392), 1003-1006.

Hauksson, E., J. Stock, R. Bilham, M. Boese, X. W. Chen, E. J. Fielding, J. Galetzka, K. W. Hudnut, K. Hutton, L. M. Jones, H. Kanamori, P. M. Shearer, J. Steidl, J. Treiman, S. J. Wei, and W. Z. Yang (2013), Report on the August 2012 Brawley Earthquake Swarm in Imperial Valley, Southern California, *Seismological Research Letters*, *84*(2), 177-189.

Kim, K. H., J. H. Ree, Y. Kim, S. Kim, S. Y. Kang, and W. Seo (2018), Assessing whether the 2017 M-w 5.4 Pohang earthquake in South Korea was an induced event, *Science*, *360*(6392), 1007-1009.

Ross, Z. et al., Hierarchical interlocked orthogonal faulting in the 2019 Ridgecrest earthquake sequence, Science, 2019.

Rutqvist, J. (2011), Status of the TOUGH-FLAC simulator and recent applications related to coupled fluid flow and crustal deformations, *Computers & Geosciences*, *37*(6), 739-750.

Smith, J. D., J. P. Avouac, R. S. White, A. Copley, A. Gualandi, and S. Bourne (2019), Reconciling the Long-Term Relationship Between Reservoir Pore Pressure Depletion and Compaction in the Groningen Region, *Journal of Geophysical Research-Solid Earth*, *124*(6), 6165-6178.

van der Elst, N. J., M. T. Page, D. A. Weiser, T. H. W. Goebel, and S. M. Hosseini (2016), Induced earthquake magnitudes are as large as (statistically) expected, *Journal of Geophysical Research-Solid Earth*, *121*(6), 4575-4590.

Wei, S., J.-P. Avouac, K. W. Hudnut, A. Donnellan, J. W. Parker, R. W. Graves, D. Helmberger, E. Fielding, Z. Liu, F. Cappa, and M. Eneva (2015), The 2012 Brawley swarm triggered by injection-induced aseismic slip, *Earth and Planetary Science Letters*, *422*, 115-125.

Zhang, Q. *et al.* Absence of remote earthquake triggering within the Coso and Salton Sea geothermal production fields. *Geophys. Res. Lett.* **44**, 726–733 (2017).